Electrochimica Acta 461 (2023) 142639

Contents lists available at ScienceDirect

Electrochimica Acta

journal homepage: www.journals.elsevier.com/electrochimica-acta

Copper-modified carbon nano-onions as electrode modifiers for the electroanalysis of the antiretroviral drug Efavirenz

K.V. Mokwebo [a,c], E. Murphy [a], S.K. Guin [a], A. Camisasca [b], S. Giordani [b], C. Breslin [a], E. I. Iwuoha [c], E. Dempsey [a,*]

[a] Department of Chemistry, Kathleen Lonsdale Institute for Human Health Research, Maynooth University, Maynooth, Kildare, Ireland
[b] School of Chemical Sciences, Dublin City University, Glasnevin, Dublin, Ireland
[c] SensorLab, Department of Chemical Sciences, University of the Western Cape, Cape Town, South Africa

ARTICLE INFO

Keywords:
Antiretroviral drugs
Efavirenz
Carbon nano-onions
Copper nanoparticles
Triple-pulse electrosynthesis
Voltammetric sensors
Wastewater influent and effluent

ABSTRACT

The high prescription and consumption rate of antiretroviral drugs (ARV) such as Efavirenz (EFV) in South Africa for the treatment of the human immunodeficiency virus (HIV) has resulted in its presence in wastewater and surface water. Herein we report the electroanalysis of EFV at oxidised boron-nitrogen doped carbon nano-onions (oxi-BNCNO) and microscale branched copper cluster (CuC) modified glassy carbon electrodes. Potentiostatic electrodeposition of CuC on the oxi-BNCNO/GCE platform resulted in a stable and electrocatalytic surface that accelerated electron transfer between the analyte and the CuC/oxi-BNCNO/GCE surface, making quantification efficient. The electroactive surface area of CuC/oxi-BNCNO/GCE was estimated as being 3 times higher than bare GCE and twice that of oxi-BNCNO/GCE. The electrooxidation of EFV on a CuC/oxi-BNCNO/GCE sensor resulted in a pH-dependant anodic peak in the potential range of 0.8 to 1.2 V vs Ag/AgCl (3M KCl). The EFV voltammetric signal increased linearly with increasing concentration of EFV in the linear dynamic range (LDR) of 0.01 – 1.0 μM and 0.5 – 20 μM with a limit of detection (LOD) and quantification (LOQ) of 1.2 and 3.97 nM, respectively. Moreover, the sensor had a sensitivity of 23 μA • cm^{-2} • μM^{-1} and was selective to 100-fold of interferents including heavy metal ions and other ARVs with the exception of high concentrations of nevirapine. The developed electroanalytical method was successfully applied for the determination of EFV in real samples such as wastewater influent and effluent, drinking/tap water, and a pharmaceutical formulation with recovery ranging from 97.8% to 109.5%.

1. Introduction

The prevalence of human immunodeficiency virus and acquired immunodeficiency syndrome (HIV/AIDS) in the African continent has led to an unprecedented awareness of the disease. This has resulted in approximately 38.4 million people testing positive for HIV/AIDS globally [1], which has subsequently led to an increase in demand and production of antiretroviral drugs (ARV), having high potency for HIV treatment and management. By the end of 2021, more than 28.7 million (75%) of those living with HIV had access to the drugs [2]. One of the ARV that is extensively prescribed is efavirenz (EFV). Once consumed, this benzoxazine compound is poorly absorbed by the body (bioavailability of 45–50%) and takes 5 hr to reach its peak plasma concentration (C_{max}) of 13 μmol L^{-1} [3–5]. The drug is further metabolised by cytochrome P450 2B6 (CYP2B6) enzymes into several hydroxy-efavirenz, with *S*-8-hydroxyefavirenz being the primary metabolite excreted [6]. Due to its widespread use in the treatment of HIV, high dosage (600 mg), low water solubility, extensive metabolism, and excretion (16–61%), and its refractory nature during wastewater treatment, it is crucial to monitor the concentration of EFV in plasma/serum, pharmaceutical formulation, and wastewater. Therapeutic monitoring of plasma levels may also assist in understanding the virologic response and in achieving optimal concentrations, thereby preventing EFV resistance and side effects [7–10], while pharmaceutical formulation monitoring can assist in quality assurance as ARV are not spared from counterfeiting, especially given their high unit costs and increasing demand for long-term treatment [11]. Moreover, EFV has been identified as an emerging environmental micropollutant due to its refractory nature against conventional wastewater treatment processes such as activated sludge and chlorination [12]. Consequently, it has been detected in wastewater [12–17],

* Corresponding author.
E-mail address: eithne.dempsey@mu.ie (E. Dempsey).

https://doi.org/10.1016/j.electacta.2023.142639
Received 30 January 2023; Received in revised form 9 May 2023; Accepted 22 May 2023
Available online 24 May 2023

surface water [14,18–20] and drinking water [18,21].

Currently, studies reported on the analysis of EFV are based on chromatographic methods [12–17,22]. As an alternative, electroanalytical methods may provide the required sensitivity and selectivity for the determination of EFV in complex sample matrices while reducing costs and analysis time. The electrochemical determination of EFV has been rarely reported, and analysis was performed only in pharmaceutical formulations and biological samples using voltammetric methods [23–28]. Initial studies on EFV electroanalysis were reported on a pencil graphite electrode (PGE) modified with DNA with adsorptive stripping differential pulse voltammetry (AdsDPV). The method produced a LOD of 1.9 μM [24] but required the use of costly biological reagents. The second study was performed by Castro et al. [23] using a thin mercury film electrode together with AdsDPV. Although the LOD was 3 nM, the toxicity of mercury limited the applicability of this approach. Therefore, the detection of EFV using electrode modifiers with high surface-to-volume, catalytic effects, excellent stability, and low toxicity to the environment are much needed. Consequently, nanomaterials such as titanium nanoparticles (TiO_2) [27], nickel oxide-zirconium oxide nanocomposite (NiO-ZrO_2) [26], and electrochemically reduced graphene oxide grafted platinum nanoparticles (ErGO-Pt NPs) [25] have been used as electrode modifiers to increase the sensitivity and stability of EFV sensors. Using NiO-ZrO_2 nanocomposite, Thapliyal et al[26] obtained a LOD of 1.4 nM with a linear range of 0.01–10 μM. The nanocomposite was prepared by chemically milling NiO and ZrO_2, resulting in an agglomerated nanocomposite which might affect the electrocatalytic activity of the nanoparticles. In this regard, a surfactant was required to decrease agglomeration. Moreover, the non-chemically bonded nanoparticles may desorb and leach during analysis. In addition, the linear range (0.01 – 10 μM) was below the reported concentration of EFV in both plasma (C_{max} = 13 μM) [3,4] and pharmaceutical tablets. Another voltammetric sensor for EFV was developed by Raj et al. [25] using an edge plane pyrolytic graphite electrode (EPGE) modified with ErGO-Pt NPs and Nafion®. The ErGO-Pt NPs improved the electrocatalytic performance of the sensor, while Nafion® improved its stability > 5 days. Nafion® was also employed in another study as a TiO_2 nanoparticle stabiliser for the voltammetric determination of EFV at the lowest concentration of 10nM [27].

Herein, oxidised boron-nitrogen codoped carbon nano-onions (oxi-BNCNO) and electrochemically synthesised microscale branched copper clusters (CuC/oxi-BNCNO) were explored as electrocatalysts in the preparation of an electrochemical sensor for the determination of EFV in wastewater and pharmaceutical formulations. The interest in the zero-dimensional, quasi-spherical and polyhedral fullerene-like carbon nano-onions arises due to their high electrical conductivity (≈ 71.8 μS), catalytic activity, large surface area, resistance to corrosion, low cytotoxicity, and their ability to form composites with other materials [29–38]. In addition, copper and its oxides have gained prominence as electrocatalysts in sensor fabrication due to their natural abundance, ease of preparation, relatively low cost, excellent electrical conductivity and electrocatalytic activity, large surface area and good reproducibility [39–42]. Mostly, copper nanoparticles used in sensor fabrication are chemically prepared (bottom-up) and then immobilised on the electrode surface by directly drop-coating the material on its surface. This may result in a weakly adsorbed catalyst that is susceptible to leaching. In order to prevent its desorption, non-conductive polymers such as Nafion® are used, resulting in a decreased electrical conductivity and electrocatalytic effect of the sensing substrate. Therefore, a one-pot metal nanoparticle electrosynthesis method for the fabrication of controllable and stable surfaces for applications in sensors and other catalytic applications are of interest. To the best of our knowledge, this study is the first of its kind, advancing the electroanalysis of this important drug molecule at novel surface architectures.

2. Experimental

2.1. Chemicals and reagents

The reference standard of efavirenz (EFV, ≥ 98%, M_r = 315.675g mol^{-1}, CAS no: 154,598–52–4), copper (II) acetate monohydrate Cu $(CH_3COO)_2.H_2O$, sodium acetate ($NaCH_3COO$), potassium phosphate monobasic (KH_2PO_4), potassium phosphate dibasic (K_2HPO_4), sodium hydroxide (NaOH), hydrochloric acid (HCl), potassium chloride (KCl) potassium hexacyanoferrate (III) ($K_3Fe(CN)_6$), potassium hexacyanoferrate (II) trihydrate ($(K_4Fe(CN)_6).3H_2O$) and potential interferents such as cadmium(II) (Cd^{2+}), chromium(VI) (Cr^{6+}), lead(II) (Pb^{2+}), copper(II) (Cu^{2+}), urea, uric acid, nevirapine (NVP), tenofovir (TNF), emtricitabine (FTC), ascorbic acid (AA), urea were purchased from Sigma Aldrich. All the chemicals employed were of analytical grade and used as received. All working solutions were prepared using double distilled water ($R \geq 18$ MΩcm) from the Milli-Q unit, Millipore. The oxi-BNCNO were synthesised based on the methods reported by Camisasca et al. [30] and provided by Prof. S. Giordani for the purposes of this work.

2.2. Real sample preparation

To evaluate the applicability of the proposed electroanalytical method for the detection of EFV in real samples, wastewater, drinking (tap) water, and Atripla tablet (an ARV tablet containing 600 mg EFV, 245 mg TNF, and 200 mg FTC) were used. Wastewater influent and effluent samples were collected from the Zandvliet wastewater treatment works (WWTW), Cape Town, South Africa, while drinking/tap water samples were collected from SensorLab polymer laboratory, University of the Western Cape, South Africa. The samples were collected in amber glass bottles and stored in the refrigerator when not in use. For wastewater analysis, the samples were spiked with known concentrations of EFV reference standard, and the pH was adjusted to 8. Thereafter, each sample was individually injected into an electrochemical cell and analysed. Due to the low conductivity of drinking water, the sample was first mixed with phosphate buffer (PB, pH 8) before analysis. For EFV analysis in the pharmaceutical tablet, one Atripla tablet (M171) weighing 1.6528 g was crushed in a mortar into finely homogenised powder. The powder was weighed (1.6133 g) and dissolved in a mixture of methanol and double distilled water by sonication and then filtered. The resultant supernatant was then diluted with 0.1 M PB (pH 8) to make 80.67 mg L^{-1} Atripla stock solution. During analysis, 0.1 μL of the stock solution was injected into an electrochemical cell containing 4 mL of PB (pH 8) and analysed before being spiked with known concentrations of the reference standard. The concentration or amount of EFV in the real samples was determined via standard addition using the differential pulse voltammetry (DPV) method.

2.3. Instrumentation

All voltammetric studies were carried out using PalmSens potentiostat (Palmsens BV, Netherlands) with PStrace software. Electrochemical impedance spectroscopy (EIS) analysis was performed on a CHI instrument (CHI 770E) electrochemical workstation. All measurements were carried out in triplicate (n = 3) and their relative standard deviations (RSD) were reported. A conventional three-electrode system having a working glassy carbon electrode (GCE, BASi MF-2012 diameter 3.0 mm), Pt wire counter electrode and Ag/AgCl (3M KCl) reference electrode (BASi) was employed for electrochemical experiments. Prior to each electrochemical experiment, the electrolyte was purged with pure nitrogen gas (N_2) to remove dissolved oxygen from the solutions. The pH of all the solutions employed was measured using a pH metre HI2211 pH/ORP metre (Hanna instruments). The morphology of the copper-carbon nanoonion nanocomposite was obtained using FEI Helio G4 CX

Dual Beam focused ion beam scanning electron microscopy (FIB-SEM) equipped with Energy dispersive X-ray (EDX) (Thermo Fisher Scientific) performed at the Bernal Institute, University of Limerick, Ireland.

2.4. Electrochemical sensor fabrication and copper nanoparticle electrodeposition

Prior to sensor fabrication and electrochemical experiments, the GCE was initially cleaned by polishing with alumina slurry to obtain a clean mirror-like surface, followed by sonication in a mixture of ethanol and deionised water (1:1) for 5 min, and dried under an infrared (IR) lamp. For sensor construction, as depicted in Scheme 1, 2 μL of oxi-BNCNO in ethanol (50 μg ·mL^{-1}) was drop-coated on the GCE and then dried under an IR lamp to construct the oxi-BNCNO/GCE modified substrate. Electrosynthesis of copper particles involved a template-free triple-pulse potentiostatic approach [43]. Briefly, the oxi-BNCNO/GCE was immersed in a 10 mM copper acetate solution prepared in sodium acetate (pH 4.5) and a potential of 0.700V was applied for 5 s to remove any pre-adsorbed Cu^{2+} *(aq)* ions. Thereafter, a potential of −0.470 V was applied for a very short period of 0.005 s to allow copper nanoparticle seeding on the GCE surface and finally, a potential of −0.265 V was applied for 50 s to allow controlled growth of seeded particles to a branch morphology driven by the diffusion of the Cu^{2+} *(aq)* ions from the bulk of moderately concentrated solution ($C_{Cu(II)} = 10$ mM). Control of size and shape can be made possible by judicious selection of nucleation and growth pulse parameters (i.e.; potential and duration) as the method builds upon prior work by Guin et al. [43,44].

3. Results and discussion

3.1. Triple-pulse potentiostatic strategy for electrosynthesis of copper clusters (CuC)

A cyclic voltammogram (CV) of 10 mM $Cu(CH_3COO)_2$ was carried out in 0.1 M $NaCH_3COO$ buffer (pH 4.5) at a bare GCE in the potential window between −1.000 and 1.000V at a scan rate of 20mV • s^{-1}. As depicted in Fig. 1A, the CV of $Cu(CH_3COO)_2$ exhibits a cathodic (E_p^c) and an anodic (E_p^a) peak at −0.194 V and 0.281 V, respectively which are due to the reduction (reaction 1) and oxidation (reaction 2) of the Cu^{2+} on the GCE surface.

$$Cu^{2+} + 2e^- \rightarrow Cu \rightarrow [E_p^c = -0.269V] \quad \text{(Reaction 1)}$$

$$Cu \rightarrow Cu^{2+} + 2e^- \rightarrow [E_p^a = 0.179V] \quad \text{(Reaction 2)}$$

The electrochemical synthesis of controlled micro-/nano-metal clusters of controlled size and morphology on an electrode surface in the absence of any structure directing chemical additives or physical templates involves critical control over the heterogeneous nucleation and growth processes. A potentiostatic triple-pulse approach towards the template-free electrosynthesis of metal nanoparticles showed an ability to deconvolute and control the above-mentioned heterogeneous nucleation and growth processes [45–47]. Hence, from past experience, three potential pulses were selected for this experiment (Fig. 1B) in such a way that the first pulse (P1) of potential (E_1) 0.700 V was applied for 5 s (t_1) immediately after the quiet time of 10 s to ensure a copper-free GCE surface. Thereafter, a short pulse (P2) of high overpotential (E_2 at −0.470V) was applied for a duration of 0.005 s (t_2) to seed sufficient copper nuclei at the active centres of the fresh GCE surface. The final pulse (P3) was responsible to control the size, shape, and morphology of the metal clusters by controlling the growth of the metal nuclei seeded during P2. In order to achieve highly branched CuC structures on the GCE, a lower overpotential (E_3 at −0.265V) of higher duration ($t_3 = 50$ s) was selected for a moderately concentrated Cu^{2+} solution ($C_{Cu(II)} = 10$ mM). During this process, branched nanostructures emerge from the copper seeds forming discrete flower-like microstructures which are well dispersed on the electrode (see surface analysis below).

Fig. 1C shows the current transients of the applied triple potentiostatic pulses (Fig. 1B) on GCE and oxi-BNCNO in an aqueous solution of 10 mM $Cu(CH_3COO)_2$ in 0.1 M $NaCH_3COO$ buffer (pH 4.5). Integrating the nucleation currents transients corresponding to P2 (inset of Fig. 1C), the amount of copper seeds formed on oxi-BNCNO and GCE was calculated as 22.3 and 111.4 pmol, respectively. This indicates that the nucleation process on oxi-BNCNO is more controlled compared to that on GCE, due to limited availability of active sites and higher overpotential of nucleation of copper seeds. Interestingly, the growth current transient of copper on oxi-BNCNO corresponding to P3 showed a small current peak (i_m) of −0.165 mA at a very short time scale ($t_m = 0.4$ s from the application of E_3) representing a very fast overlap of diffusion zones of Cu^{2+} ions around copper seeds (Fig. 1D). However, the same process became much more intense ($i_m = -0.423$ mA), but at a longer time scale ($t_m = 1.3$ s from the application of E_3) on GCE. Therefore, a different growth mechanism of CuC on oxi-BNCNO and GCE was anticipated. Comparing the corresponding plots of $(i/i_m)^2$vs. t/t_m with the Scharifker and Hills model for instantaneous (Eq. (1)) and progressive (Eq. (2)) 3D growth [48], two different types of three-dimensional diffusion-controlled growth processes of the copper seeds on GCE and oxi-BNCNO surfaces were evident; where CuC grew on oxi-BNCNO more

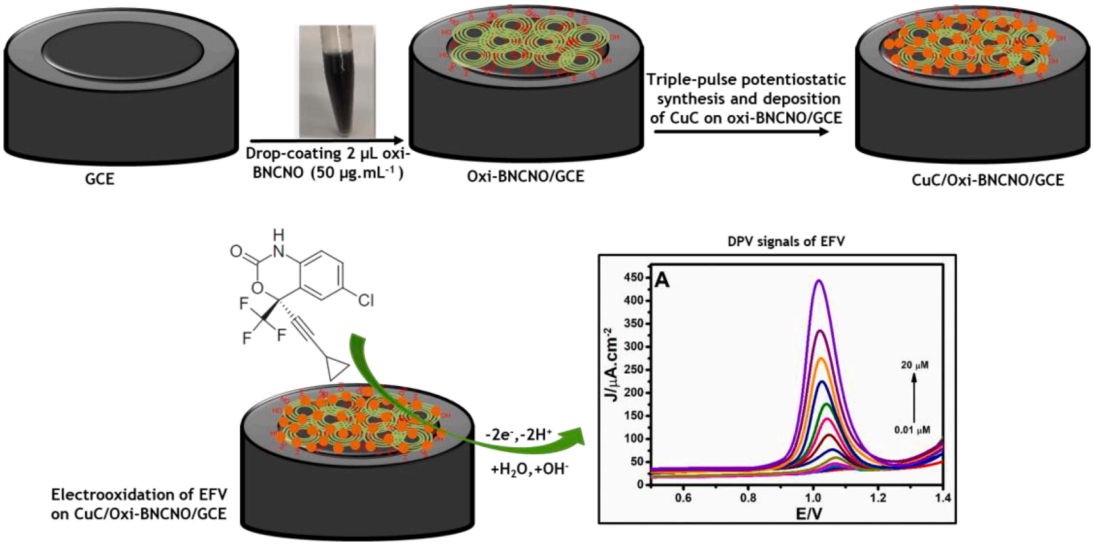

Scheme 1. Schematic representation for the fabrication of CuC/Oxi-BNCNO/GCE sensing platform for voltammetric determination of EFV.

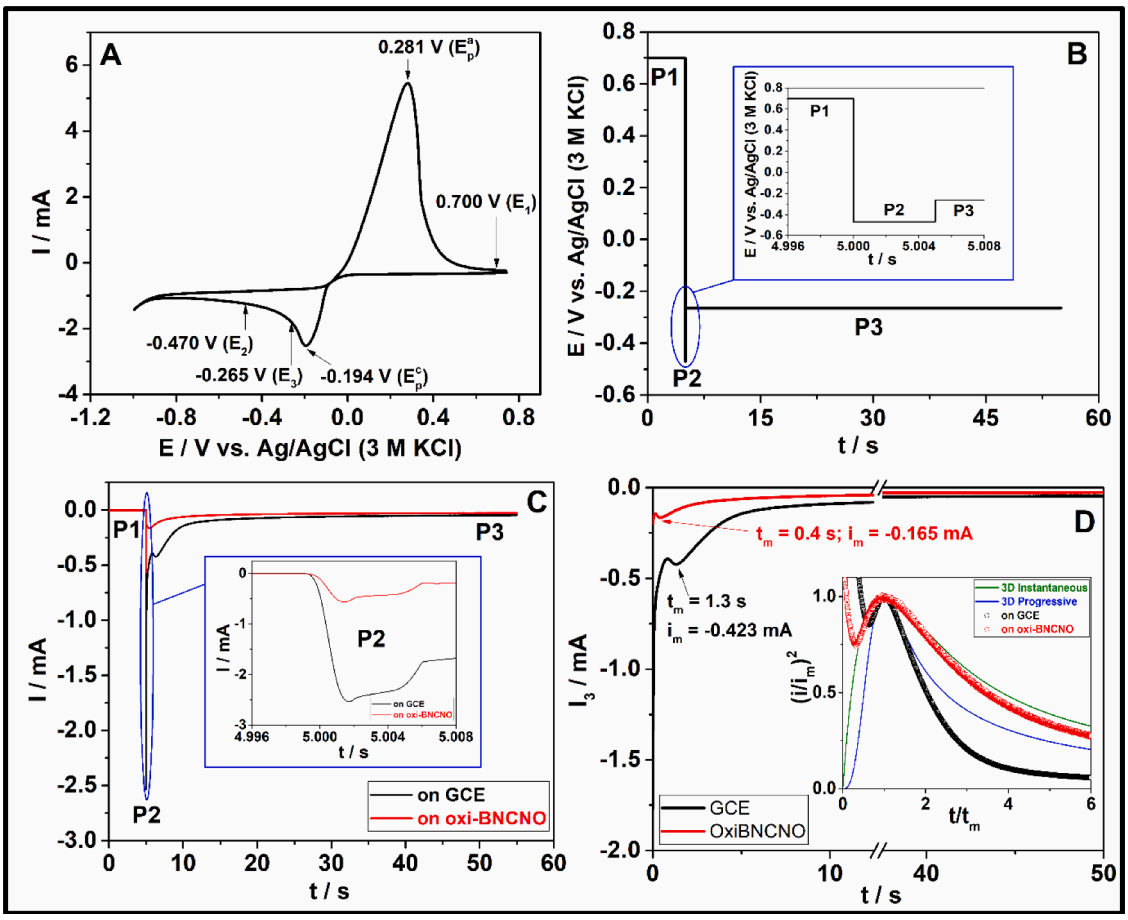

Fig. 1. CV of 10 mM $Cu(CH_3COO)_2$ in deaerated 0.1 M $NaCH_3COO$ buffer (pH 4.5) at a bare GCE at a scan rate of 20 mV•s^{-1} (A). Triple potentiostatic pulse approach (B). Current transients recorded during the application of B on oxi-BNCNO/GCE and GCE; Inset: Magnified portion of P2 (C). Current transients recorded (circles) and fitted (line) during the application of P3 on oxi-BNCNO/GCE and GCE; Inset: Corresponding $(i/i_m)^2$vs. t/t_m plots overlapped on the theoretically calculated currents following 3D instantaneous and progressive growth model of Scharifker and Hills.

instantaneously, but grew progressively on GCE (inset of Fig. 1D).

$$\left(\frac{I}{I_m}\right)^2_{Instantaneous} = 1.9542\left\{1 - exp\left[-1.2564\left(\frac{t}{t_m}\right)\right]\right\}^2\left(\frac{t}{t_m}\right)^{-1} \quad (1)$$

$$\left(\frac{I}{I_m}\right)^2_{Progressive} = 1.2254\left\{1 - exp\left[-2.3367\left(\frac{t}{t_m}\right)^2\right]\right\}^2\left(\frac{t}{t_m}\right)^{-1} \quad (2)$$

The mechanism of instantaneous growth of CuC on Cu-seeds developed on oxi-BNCNO and GCE was studied in more detail by fitting the corresponding experimental growth current transients (as shown in Fig. 1[D]) to the theoretical current ($i_{Theo.}$) calculated by using three-dimensional (3D) hemi-spherical growth model developed independently by Mirkin and Nilov[49] as well as Heerman and Tarallo[50] as expressed in Eq. (3)[45].

$$i_{Theo} = i_{DL} + i_{IT} + i_{3D} \quad (3)$$

where, i_{DL} (Eq. (4)) and i_{IT} (Eq. (5)) represent the current components of double-layer rearrangement and ion-transfer, respectively.

$$i_{DL} = K_1 * exp\left(-\frac{t}{K_2}\right) \quad (4)$$

$$i_{IT} = K_3 * exp\left(-\frac{t}{K_4}\right) \quad (5)$$

Where, K_1, K_3 are pre-exponential factors and K_2 and K_4 are the corresponding time constants. The 3D growth current is expressed by Eq. (6).

$$i_{3D} = nFAC_0 * \sqrt{\frac{D}{\pi t}} * \left[\frac{\Phi}{\Theta}\right] * [1 - \exp(-\pi\Theta D N_0 k' t)] \quad (6)$$

Where,

$$\frac{\Phi}{\Theta} = \frac{\left[1.185724(at)^2 - 1.206814(at)^{1.5} + 0.520893(at) - 0.051314(at)^{0.5}\right]}{\left[\{at - 1 + \exp(-at)\}\left\{1 + 1.185724(at) - 1.206814(at)^{0.5}\right\}\right]} \quad (7)$$

$$\Theta = 1 - \left(\frac{1 - \exp(-at)}{at}\right) \quad (8)$$

$$k' = \sqrt{\frac{8\pi C_0 M}{\rho}} \quad (9)$$

where, z, F, A, C_0, D, M and ρ are number of electrons per ion involved in the reduction process (here $z = 2$), Faraday constant (96,485 C mol^{-1}), electrode area (0.07 cm^2), concentration of $Cu(CH_3COO)_2$ (1×10^{-5}mol·cm^{-3}), diffusion coefficient (D) of Cu(II) ($cm^2 \cdot s^{-1}$), atomic weight of Cu (63.5 g ·mol^{-1}) and density of Cu (9 g·cm^{-3}), respectively. N_0 (cm^{-2}) and a (s^{-1}) represent the density of new growth site formation and the rate of growth, respectively. The best fitted theoretical current transients were overlaid on the experimental current transients in Fig. 1 [D] and the fitted parameters are shown in Table 1. It can be seen that the growth rate (a) of CuC on oxi-BNCNO (5.5 s^{-1}) was very high

Table 1
3D growth parameters of CuC on Cu-seeds nucleated on oxi-BNCNO and GCE.

Parameters	During growth on oxi-BNCNO	During growth on GCE
K_1 (A)	6.6×10^{-5}	1.1×10^{-3}
K_2 (s)	0.06	0.03
K_3 (A)	1.3×10^{-4}	7.5×10^{-4}
K_4 (s)	0.5	0.5
N_0 (cm^{-2})	5.7×10^{6}	1.0×10^{6}
a (s^{-1})	5.5	0.8
D ($cm^2\ s^{-1}$)	3.0×10^{-6}	2.7×10^{-5}
$\chi 2$	4.7×10^{-13}	3.9×10^{-10}
Adj. R^2	0.9994	0.9824

compared to that on GCE (0.8 s^{-1}) for growing almost same number of growth centres (~10^6 cm^{-2}). Thus, the distinct microstructure of CuC was developed on oxi-BNCNO due to instantaneous growth of copper (during growth pulse) on a highly limited number of seeds produced during the nucleation pulse.

3.2. Physicochemical characterisation of CuC/oxi-BNCNO/GCE

The morphological characterisation of the prepared sensing substrate was investigated using focused ion beam scanning electron microscopy (FIB-SEM) coupled with energy diffraction X-ray (EDX) with a specially fabricated electrode holding stage. The FIB-SEM image in Fig. 2B-C depicts the dense flower-like morphology of the metal nano/microstructures on the oxi-BNCNO modified GCE with the majority being <1 μm with nanoscale projections and some clustering evident in regions [30,51,52]. EDX mapping and elemental analysis were also performed (Fig. 2D-E), where copper in addition to oxygen was evident due to possible surface oxidation (CuO/Cu_2O) of highly reactive copper nano/microstructures and the contribution from the oxygenated groups of the BN doped CNO materials. The high percentage of carbon in EDX is due to the GCE substrate and the oxi-BNCNO. The CuC/oxiBNCNO/GCE was prepared on a commercial BASi MF-2012 glassy carbon column electrode under optimised drop-casting and electrodeposition conditions. Any post-treatment (such as sonication to cast on a grid) or change of electrode type to carbon tape/paper (having different overpotentials)

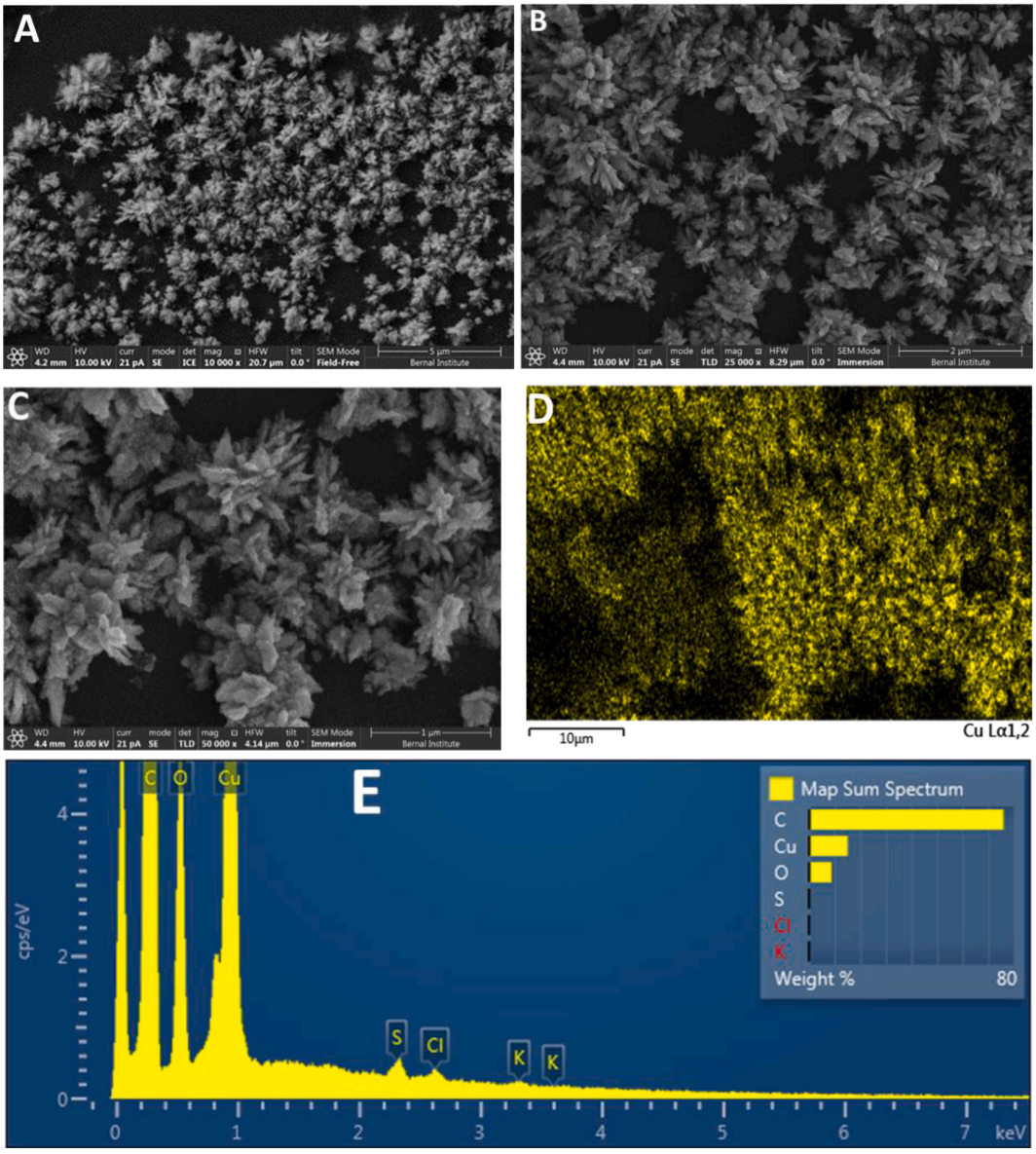

Fig. 2. FIB-SEM images of (A), CuC/oxiBNCNO/GCE at 5 μm (B) 2 μm (C) 1 mm magnification scales with EDS mapping (Cu) and elemental analysis (D, E) of CuC/BNCNO/GCE.

would risk results different to those prepared here. Hence, no further characterisation of the modified electrode was carried out through transmission electron microscope or x-ray photoelectron spectroscopy.

3.3. Electrochemical characterisation of CuCs/oxi-BNCNO/GCE

To examine the electrochemical properties of each of the layers immobilised on the GCE surface during sensor fabrication, CV and EIS analysis were performed in 0.1 M KCl containing 5 mM $[Fe(CN)_6]^{3-/4-}$ redox probe. As depicted in Fig. 3A, the CV of GCE exhibited two reversible redox peaks at $E_p^a = 0.473$ V and $E_p^c = -0.041$ V with a peak-to-peak separation (ΔE_p) of 0.514 V. Compared to GCE, the redox probe in oxi-BNCNO/GCE exhibited well-defined redox peaks with higher peak currents and a lower ΔE_p of 0.151 V. The high electrocatalytic activity demonstrated by the oxi-BNCNO may be attributed to the increased porosity and surface area of the modified electrode. The high porosity facilitated faster diffusion and electron transfer of the redox probe to the surface [53]. Furthermore, the highly conductive multishell fullerene may create a bridge to accelerate electron transfer between $[Fe(CN)_6]^{3-/4-}$ and oxi-BNCNO/GCE [54,55]. The modification of oxi-BNCNO/GCE with copper further increased the peak intensity of the redox probe and slightly reduced ΔE_p to 0.097 V. The electroactive surface area (A_{eff}) of GCE, oxi-BNCNO/GCE, and CuC/oxi-BNCNO/GCE were estimated as 0.0619, 0.1135 and 0.205 cm^2, respectively, using the Randles-Sevcik (Eq S.1) and the slope of Fig. S. 1. Furthermore, the surface coverages (Γ)[10] of oxiBNCNO/GCE and CuC/oxiBNCNO/GCE were calculated as 9.96 and 17.14 $nmol^{-1} \cdot cm^{-2}$, respectively, using Eq. S.2 and the slope of 0.664 and 1.143 $\mu A \cdot mV^{-1}$ of the I_{pa} vs. υ plots in Fig. S. 1.

To further examine the impedance characteristics of the modified electrodes, Nyquist plot parameters were obtained by fitting the EIS analysis data with an equivalent Randles circuit. Fig. 3B displays the obtained and fitted Nyquist plots of oxi-BNCNO/GCE, and CuC/oxi-BNCNO/GCE when characterised in 5 mM $[Fe(CN)_6]^{3-/4-}$ in 0.1 M KCl, while Fig. 3B insert depicts the fitted Nyquist plot of GCE. The charge transfer resistance (R_{CT}) of any material is influenced by the dielectric and insulating properties of the electrode and electrolyte solution. As depicted in Fig. 3B and Table 2, the R_{CT} of GCE was 13 times and 124 times larger than that of oxi-BNCNO/GCE and CuC/oxi-BNCNO/GCE, respectively. The low R_{CT} in the presence of oxi-BNCNO indicates that the modified electrode had an excellent electron conductance pathway for electron exchange between the redox probe and the transducing element. The absence of Warburg diffusion in the GCE Nyquist plot indicated that the diffusion of the redox probe was restricted. This may be due to limited active surface area and also the repulsive force between the negatively charged GCE surface and the

Table 2
EIS parameters for GCE, Oxi-BNCNO/GCE, CuC/oxi-BNCNO/GCE after fitting the Nyquist plots with equivalent circuits.

Electrode	$E_{1/2}$ (V)	R_s (Ω)	R_{ct} (Ω)	CPE1-T (μF)	CPE1-P (μF)	k_{app} ($cm\ s^{-1}$)	θ (%)
GCE	0.186	82	7528	8.86×10^{-6}	0.74	1.14×10^{-4}	n/a
BNCNO/GCE	0.191	91	560	1.76×10^{-5}	0.67	8.37×10^{-4}	92.6
CuC/oxi-BNCNO/GCE	0.123	102	61	3.4×10^{-6}	0.98	4.29×10^{-3}	99.2

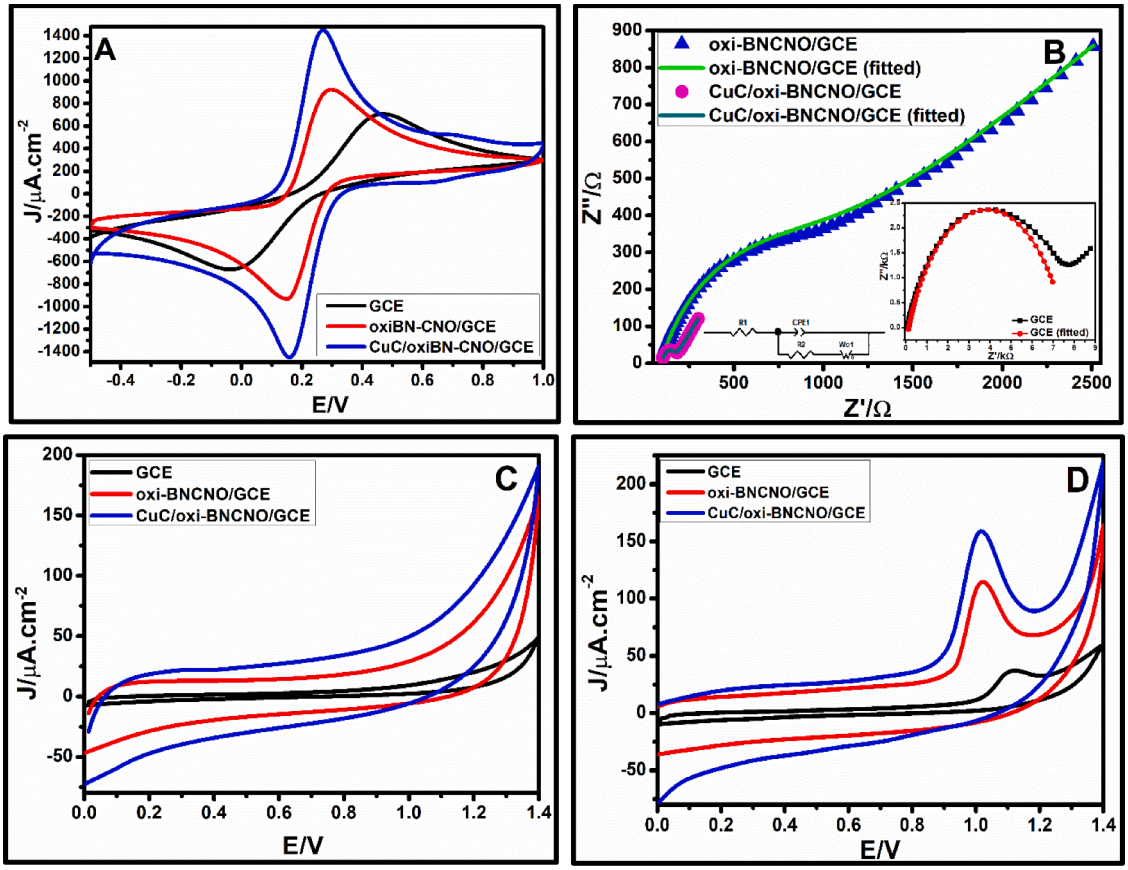

Fig. 3. CV (A) and Nyquist (B) plots of GCE, oxi-BNCNO/GCE, CuC/oxi-BNCNO/GCE in 5 mM $[Fe(CN)_6]^{3-/4-}$/0.1 M KCl redox probe at a scan rate of 50 mV s^{-1} and frequency of 10 kHz to 1.0 Hz. CV of GCE, oxi-BNCNO/GCE, and CuC/oxi-BNCNO/GCE in 0.1 M PB (pH 8) in the absence (C) and presence (D) of 10 μM EFV in the potential range of 0 to 1.4 V at 50 mV s^{-1}.

negatively charge redox probe. The apparent charge transfer rate constant (k_{app}) [56] of GCE, oxi-BNCNO/GCE, and CuC/oxi-BNCNO/GCE was determined as 1.14× 10^{-4}, 8.37× 10^{-4} and 4.29× 10^{-3} cm• s^{-1}, respectively using Eq. 10 [56].

$$k_{app} = \frac{RT}{n^2F^2A_{eff}R_{CT}C_o} \quad (10)$$

where R is the gas constant (8.314 $J\,K^{-1}$• mol^{-1}), T is the temperature (298 K), F is Faraday's constant (96,485 C•mol^{-1}), n is the number of electrons transferred, A_{eff} is the effective surface area obtained using Randles-Sevcik equation in (S1) and C_o is the concentration of the bulk redox probe (5 µmol• cm^{-3}). At low R_{CT} values, k_{app} was higher, indicating that the modification of the electrodes with the nanomaterials resulted in an accelerated electron transfer rate between the electroactive species and the electrode surface. Moreover, the partial surface coverage (θ) [56] of the GCE by the electrode modifiers was determined using equation (Eq. (11)) [56].

$$\theta = 1 - \frac{R_{CT}}{R^0_{CT}} \quad (11)$$

where R^0_{CT} and R_{CT} are the charge transfer resistance of the bare GCE and the modified GCE, respectively. The redox probe covered 92.6% and 99.2% of the oxi-BNCNO/GCE and CuC/oxi-BNCNO/GCE platforms, respectively.

In phosphate buffer (PB, pH 8) with potential range of 0 to 1.4 V, the GCE, oxi-BNCNO/GCE and CuC/oxi-BNCNO/GCE do not show any redox activity. However, the capacitive current increased in the presence of the oxi-BNCNO and CuC (Fig. 3C), due to the high electrical conductivity of the nanocomposites. To investigate the sensing ability of the developed CuC/oxi-BNCNO/GCE substrate towards EFV, the electrochemical behaviour of the various modified electrodes in the absence and presence of 10 µM EFV in 0.1 M PB (pH 8) was investigated. As depicted in Fig. 3D, on a bare GCE, EFV exhibited an irreversible oxidation peak at E^a_p = 1.120 V vs Ag/AgCl with a current of 2.17 µA. Upon modification with oxi-BNCNO, the EFV signal increased to 7.89 µA with a negative shift in potential (E^a_p = 1.012 V). The increase in current and decrease in potential energy in oxi-BNCNO/GCE indicated that the porous and highly conductive oxi-BNCNO was electrocatalytic towards EFV. Under the conditions examined (pH 8), the EFV species (pK_a 10.2) may interact with the anionic oxi-BNCNO surface, leading to potential adsorption and accelerated electron transfer rate. Although the

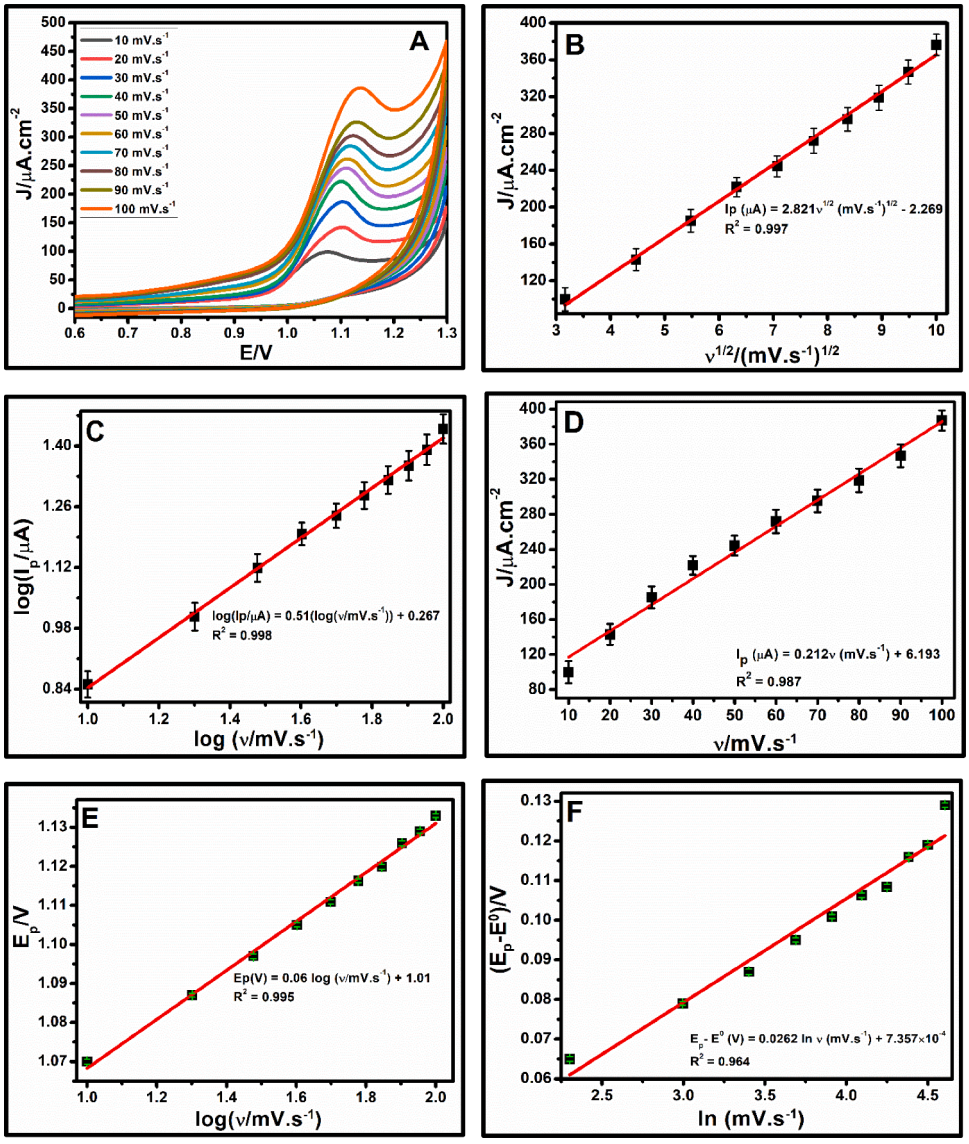

Fig. 4. Cyclic voltammogram of CuC/oxi-BNCNO/GCE in PB (pH 8) containing 10 µM of EFV at various scan rates (10–100 mV s^{-1}) [A], Regression plots of I_p vs $\upsilon^{1/2}$ [B], log (I_p) vs log (υ) [C], I_p vs υ [D], E_p vs log (υ) [E], and (E_p – E^0) vs ln (υ) [F].

capacitive current of oxi-BNCNO/GCE was slightly higher, it did not affect the sensitivity of the sensing substrate. To further amplify the EFV signal, the CuC/oxi-BNCNO/GCE surface was examined in relation to the EFV response. The electrosynthesis of copper particles onto the carbon nano-onion surface enhanced the anodic peak current of EFV further to 11.45 μA, while the peak potential did not change. The lack of electrocatalytic effect may be due to the repulsive force between the positively charged Cu and the positively charged benzoxazine ring of EFV at pH 8. Moreover, the formation of the insoluble $Cu(OH)_2$ and CuO layers on the electrode surface may play a role. However, due to the high conductivity and large surface area of the branched Cu deposits, the current signal of EFV was distinctive and enhanced, encouraging further studies.

3.6. Effect of scan rate on EFV signal on a CuC/oxi-BNCNO/GCE

To further study the electrochemical dynamics of EFV on the CuC/oxi-BNCNO/GCE sensor, scan rate (υ) studies from 10 to 100 mV· s^{-1} were performed. Fig. 4A depicts the CV of CuC/oxi-BNCNO/GCE in PB (pH 8) containing 10 μM EFV. The I_p^a of EFV increased with υ, while the E_p^a shifted positively with increasing υ. The absence of a reduction peak and the positive shift in E_p^a with increasing υ indicates that the electro-oxidation of EFV at CuC/oxi-BNCNO/GCE was irreversible. As shown in Fig. 4B, the plot of I_p^a vs $\upsilon^{1/2}$ resulted in a linear plot with $R^2 = 0.997$, suggesting that the electron transfer process at the CuC/oxi-BNCNO/GCE was diffusion-controlled. The plot of log (I_p^a) vs. log (υ) in Fig. 4C was also linear ($R^2 = 0.998$) with a slope of 0.51, being close to the theoretical value (0.5) for diffusion-controlled reactions. The diffusion coefficient (D) of EFV on CuC/oxi-BNCNO/GCE was calculated as 5.296×10^{-3} $cm^2 \bullet s^{-1}$ using the Nicholas-Shain equation (modified Randle-Sevcik equation) [57] in Eq. (12) for irreversible processes.

$$I_p^a(\mu A) = 2.99 \times 10^5 n(\alpha n_\alpha)^{1/2} A_{eff} D^{1/2} C_o \upsilon^{1/2} \left((mVs^{-1})^{-1/2} \right) \quad (12)$$

where α is the charge transfer coefficient, which is assumed to be 0.5 for a diffusion-controlled reaction, C_o is the concentration of the analyte (10 μM), n is the number of electrons involved in the irreversible reaction (~2 using Eq. (13)), A_{eff} is the effective surface area of CuC/oxi-BNCNO/GCE (0.205 cm^2).

The dependency of E_p on υ was investigated and according to Laviron's equation for irreversible reactions [58], the slope of the regression curve of E_p vs. log υ can be used to determine the number of electrons (n) transferred during the electro-oxidation process. Moreover, the intercept of that plot results in the reduction formal potential (E^0) of the electroactive compound - Fig. 4E with the regression equation (Eq. (13)) [58–60] below for 10 μM EFV.

$$E_p = E^0 + [2.3RT / (1-\alpha) n_\alpha F] \log \upsilon \quad (13)$$

where E^0 is the formal potential ($E^0 = 1.010V$), R is the gas constant ($8.314 J K^{-1}$ mol^{-1}), T is the temperature (298K), F is Faraday's constant (96,485 C mol^{-1}), n_α is the number of electrons transferred and α is the electron-transfer coefficient. Having a slope of 0.06 and assuming α to be 0.5 for a diffusion-controlled reaction, the number of electrons involved at pH 8 was calculated as 1.96 ($n \approx 2$). Although α was initially assumed, it can be estimated using the Laviron equation [58,60,61] Eq. (14) and the slope (0.0603) of the plot in Fig. 4F. The value of α was calculated as 0.5099 (≈ 0.51), which is in agreement with the theoretical value of α for diffusion-controlled reactions. The charge transfer rate constant (k_{ct}) was also calculated using the intercept of Eq. (14) and was determined as 37.082 s^{-1}.

$$E_p - E^0(V) = RT/(1-\alpha) n_\alpha F . \ln((1-\alpha) n_\alpha F / RTk_{ct}) + RT/(1-\alpha) n_\alpha F \ln(v / (mVs^{-1})) \quad (14)$$

3.5. Effect of pH on the electrochemical behaviour of EFV at CuC/oxi-BNCNO/GCE

The pH of the supporting electrolyte may affect the peak position and signal strength of an electroactive compound when protons are involved in the redox process and varying the pH of the supporting electrolyte during the electro-oxidation of an electroactive species can provide significant information about the electrochemical mechanisms involved. Therefore, the pH dependency of 10 μM EFV at the CuC/oxi-BNCNO/GCE sensor was investigated over the range 5 to 12 (0.1 M PB electrolyte) using differential pulse voltammetry (DPV). As displayed in Fig. 5A, EFV exhibited only one irreversible oxidation peak from pH 5 to 12 in the potential window of 0.500 to 1.400 V. These well-defined oxidation peaks shifted cathodically with increasing pH, and the peak current increased from pH 5 to 8, and then decreased thereafter. Fig. 5B shows line graphs of pH vs. I_p^a and E_p^a. The highest I_p^a of EFV was observed at pH 8 with E_p^a of 1.010V and I_p^a of 13.79 μA. The negative linear shift of E_p^a from 1.200 to 0.850 V with increasing pH was also observed as shown in Fig. 5B resulting in two Nernstian ranges [10,62,63] over pH 5–9 and 10–12 with slopes of 60.1 and 33.7 mV·$decade^{-1}$, respectively (Fig. 5C and D). The regression curves of the two plots had the following equations:

$$E_p^a\ (V) = -0.0601pH + 1.503 (R^2 = 0.9996); (pH5 - 9) \quad (15)$$

$$E_p^a\ (V) = -0.0337pH + 1.260 (R^2 = 0.9940); (pH10 - 12) \quad (16)$$

According to Nernst's theory, a slope of −0.0601 V• pH^{-1} as shown in Eq. (15), which is closer to the Nernstian value of −0.059 V•pH^{-1} suggests that an equal number of protons and electrons were participating in the electro-oxidation of EFV at the CuC/oxi-BNCNO/GCE substrate. The slope of −0.0337 V•pH^{-1} (Eq. (16)), which is closer to −0.03 V•pH^{-1} indicates that an unequal number of electrons and protons were participating over this range (> pH 10). Although the literature reported a pK_a of 10.2 for EFV [64], the intersection of E_p vs pH for the two regression curves was calculated as 9.2 on this modified electrode, which may be due to drug-metal interactions which lower the basicity of the EFV resulting in a decrease in the peak current of EFV at this pH value as shown in Fig. 5A. Although the number of electrons and protons involved were estimated as 2 using Eq. (13) and Eq. (15), this work does not focus on direct clarification of the detailed mechanism of the electrooxidation of EFV, which requires potentiostatic or galvanostatic coulometric analysis for total electrooxidation and conversion of the analyte. Nevertheless, Thapliyal et al. [26] and Mthiyane et al. [27] have proposed a one electron and one proton electrooxidation mechanism involving the benzoxazine ring to produce a free nitrogen radical at the benzoxazine ring, resulting in possible dimers. Since EFV was first dissolved in methanol and added to an alkaline medium before electrooxidation, the drug molecule may also undergo alkaline hydrolysis to an amino alcohol product which may subsequently undergo electro-oxidative dehydration and cyclisation on the CuC/oxi-BNCNO/GCE surface to give a quinoline product [65–67]. Such impurities may account for altered pH dependence > pH 10 which appears to manifest in a more facile electrooxidation with broadening of the wave (Fig. 5A). Hence, it was understood that at pH 8, which was selected for the following electroanalytical studies, the electrooxidation of EFV happens through the nitrogen-centre of the benzoxazine ring producing a nitrogen radical for the following dimerisation reaction, being facilitated by either Cu clusters or insoluble copper species i.e. CuO/Cu_2O due to a local pH change at the interface during the oxidation cycle. Hence, a detailed mechanistic study on electrooxidation of EFV on copper involving e.g. x-ray photoelectron spectroscopy, rotating ring-disk electrode, flow cell hyphenated with chromatography, etc. would be required for further elucidation, being out of the scope of the present study.

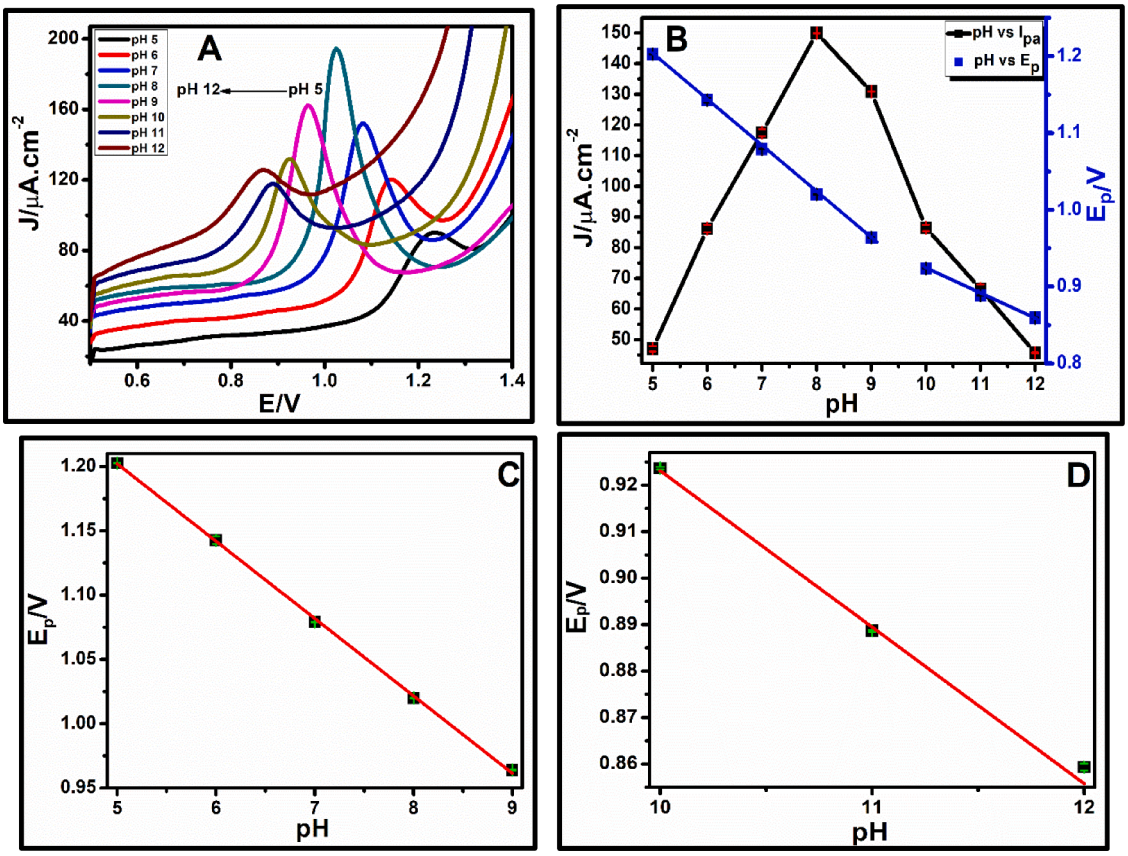

Fig. 5. DPV of 10 μM EFV in 0.1 M PB of various pH (pH 5 to 12) (A). A plot of pH vs E_p and pH vs I_p (B). Corresponding Nernst plot at pH 5–9 (C) and pH 10–12 (D).

3.7. Analytical applicability of CuC/oxi-BNCNO/GCE voltammetric sensor

To evaluate the analytical performance of CuC/oxi-BNCNO/GCE to quantitatively detect EFV in a neutral environment, DPV of 0.1 M PB (pH 8) containing EFV from 0.01 to 20 μM were recorded. Lower concentrations were chosen because EFV and other ARV exist at very low concentrations in environmental samples (ng• L^{-1} to μg• L^{-1}). As depicted in Fig. 6A and B, the oxidation peak current of EFV gradually increased with increasing concentration of EFV. At lower concentrations (0.01 – 0.50 μM), the peak potential of EFV was approximately 1.080 V with a slight cathodic shift at high concentrations. The shift in peak potential may relate to Cu-EFV (benzoxazine ring) interactions, where at lower concentrations a monolayer of EFV may be adsorbed onto the high surface-to-volume ratio layer. Indeed, preliminary data has indicated a sharp decrease in the peak intensity of the $Cu^{2+/1+}$ reduction process at −0.210 V (Fig. S.2A (v)) with increasing EFV (5–60 mM additions) confirming that the metal particles play a role in the surface-drug interactions.

The analytical response of the CuC/oxi-BNCNO/GCE sensor towards EFV generated two linear calibration curves at 0.01 – 1.0 μM Fig. 6C) and 0.50 - 20 μM (Fig. 6D) with the following linear regression equations Eq. (17) and ((18).

$$I_p^a\ (\mu A) = 4.714C(\mu M) + 1.167\left(R^2 = 0.985\right), 0.01 - -1.0\mu M \quad (17)$$

$$I_p^a\ (\mu A) = 1.107C(\mu M) + 3.35\left(R^2 = 0.986\right), 0.50 - 20\mu M \quad (18)$$

The slope of Eq. (17) together with the standard deviation of the blank (σ = 0.00187 μA) were used to calculate the limits of detection (LOD = ((3 × σ)/slope) and quantification (LOQ = (10 × σ)/slope) [68]. The LOD and LOQ of the CuC/oxi-BNCNO/GCE sensor were determined as 1.2nM (0.379 μg•L^{-1}) and 3.97nM (1.25 μg•L^{-1}), respectively and the sensitivity was calculated as 23 μA• cm^{-2} • μM^{-1}.

The performance of the developed CuC/oxi-BNCNO/GCE sensor towards the detection of EFV was compared to that of reported electrochemical sensors employed for analysing EFV in biological samples and pharmaceutical formulations. As presented in Table 3, the CuC/oxi-BNCNO/GCE sensor exhibited lower LOD compared to other reported sensors with the exception of the GCE/GO/AgNPs/AmmDCA sensor. Low LOD and linear dynamic ranges (LDR) are important in wastewater analysis as micropollutants exist at trace levels in wastewater. The excellent analytical validation parameters (LOD and LDR) observed when using the developed sensor may be due to the utilisation of the highly porous and nanometric oxi-BNCNO which created a large active surface area on the GCE, thereby allowing the adsorption of the electroactive EFV, bringing it closer to the electrode surface before electrooxidation. Moreover, the oxi-BNCNO provides a large surface area for the immobilisation of copper, thereby further increasing the active surface area and the electrocatalysis of EFV due to their synergistic effect. Finally, the use of a facile electrodeposition approach for copper particle formation and growth resulted in a stable, controllable surface which facilitated EFV electroanalysis [54]. Because this sensor was predominantly employed for the analysis of EFV in wastewater, the performance of the sensor was also compared with the reported validation parameters of the liquid chromatography coupled with the mass spectroscopy (LC-MS/MS) method that was employed for EFV analysis in water samples. As depicted in Table 4, the validation parameters were comparable to those reported using LC-MS/MS.

3.8. Effect on interferents

Prior to real sample analysis, the effect of potentially interfering compounds that may coexist with EFV in wastewater and ARV tablet were examined in the presence of 10 μM EFV (~ 3.157 μg• mL^{-1}) under

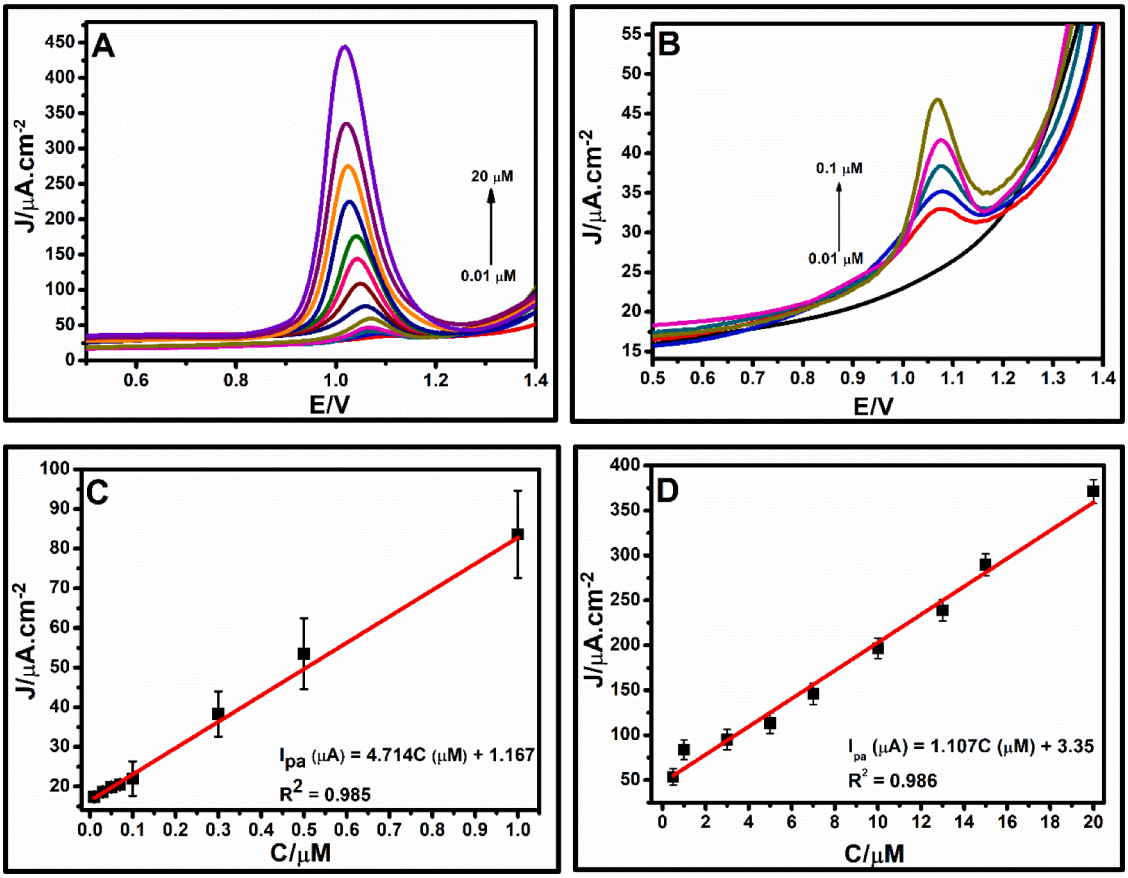

Fig. 6. DPV of CuC/oxi-BNCNO/GCE in 0.1M PB (pH 8) containing 0.01–20μM EFV (A) and enlarged DPV at lower EFV concentration (0.01–0.1μM) (B). Corresponding calibration curves for 0.01–1μM EFV (C) and 0.5–20μM EFV (D).

Table 3
A comparison of electrode material and electrochemical methods reported for the determination of EFV in different samples.

Electrode material	Method	E_p (V) and pH	Linear range	LOD	LOQ	Sample matrix	Ref.
Thin Hg film	AdSV	N/A	31.7 −792 nM	3 nM	n/a	N/A	[23]
dsDNA/PGE	AdsDPV	1.25, pH 7	6.33 – 76 μM	1.9 μM	n/a	Pharmaceutical formulation	[24]
ErGO-Pt/Nafion/EPPG	SWV	1.106, pH 7	0.05 −150 μM	1.4 nM	6.0 nM	Pharmaceutical, urine and plasma	[25]
NiO–ZrO_2/GCE	CV	1.20, pH 7	0.01 – 10 μM	1.8 nM	n/a	Pharmaceutical formulation and human urine	[26]
Nafion-TiO_2–NPs/GCE	DPV	1.01, pH 7	4.5 – 18.7μM	0.01 μM	n/a	Pharmaceutical formulation	[27]
GCE/GO/AgNps/ AmmDCA	DPV	-0.375, pH 10	1.0 to 7.0 μM	0.0474 nM	0.158 nM	Pharmaceutical formulation	[28]
CuC/oxi-BNCNO/GCE	DPV	1.02, pH 8	0.01 to 20 μM	1.2 nM	3.97 nM	Tap water, Wastewater influent and effluent, pharmaceutical formulation	This work

AmmDCA: 1-Allyl-3- methylimidazolium dicyanamide ionic liquid.

the same experimental conditions. Fig. 7A and B show the DPV and the corresponding bar graph of 10 μM EFV in the presence of 500 μM of lead (Pb^{2+}), copper (Cu^{2+}), chromium (Cr^{6+}) and cadmium (Cd^{2+}), being heavy metals that are commonly detected in wastewater. The bar graph shows that the presence of 500 μM Cd^{2+} and Pb^{2+} decreased the EFV signal by more than 50% and 20%, respectively. This may be due to the formation of chelating complexes between the small divalent ions and EFV molecule, possibly at the O, N sites. The effect of Cu^{2+} was less than ± 5%, therefore it was negligible. In the presence of Cr^{6+}, the EFV signal slightly increased by ± 9%, as chromium (VI) is an excellent oxidising agent, hence it oxidised EFV further, thereby increasing electron flow. Although levels of 500 μM Cd^{2+} and Pb^{2+} had significant effects on the voltammetric signal of EFV, metal ions do not exist at such a very high concentration in wastewater. Therefore, studies on the effect of lower concentration (50 μM) of the metal ions on the signal of 10 μM EFV were also investigated. As depicted in Fig. S. 4, the effect of metal ions on the EFV signal was negligible as the relative error for all the ions was less than ± 5%. In any case, the effect of these heavy metals can be mitigated or eliminated by introducing ethylenediaminetetraacetic acid (EDTA) to the sample before EFV analysis as a chelating agent [69].

In the pharmaceutical formulation of HAART, EFV is usually co-formulated with tenofovir (TNF) and emtricitabine (FTC) and sold

Table 4
A comparison of the study validation parameters to other analytical methods reported for the determination of EFV in environmental samples.

Analytical method	Linear dynamic range	LOD	LOQ	Sample matrices	ref
LC-MS/MS	20 – 200ng L^{-1}	7.8 ng L^{-1}	25.9 ng L^{-1}	wastewater	[12]
LC/MS-MS	10 – 5000ng L^{-1}	9 ng L^{-1}	31 ng L^{-1}	wastewater	[13]
LC-MS/MS	10 – 700μg L^{-1}	0.16 μg L^{-1} 0.113 μg L^{-1}	0.53 μg L^{-1} 0.38 μg L^{-1}	wastewater Surface water	[17]
LC-MS/MS	n/a	0.09 μg L^{-1}	0.3 μg L^{-1}	Surface and groundwater	[19]
DPV with CuC/oxi-BNCNO/GCE	3.16 -. 31.57μg L^{-1}	0.379μg L^{-1}	0.52 μg L^{-1}	Wastewater influent and effluent, and tap water	This work

under the brand name Atripla. Moreover, EFV is used interchangeably with NVP as both drugs have similar effects in suppressing the virus. Therefore, the effect of 100 μM of these drugs on the EFV signal was also investigated. In the chosen experimental conditions, TNF was oxidised at a potential of 1.320 V with low current intensity. This potential was higher than that of EFV (E_p^a = 1.030 V), thus its effect was deemed insignificant (relative error of 4.3%). FTC was also electrooxidised at a very high potential (E_p^a ~1.7V), and its effect on TNF was less than 2%. These data suggest that EFV, FTC and TNF can be simultaneously and selectively detected in various samples without interfering with each other using the prepared sensor. However, since NVP and EFV have almost similar chemical properties, NVP was able to affect the EFV signal as shown in Fig. 7C and D due to overlapping signals. NVP was electrooxidised at 1.22 V while EFV was oxidised at 1.05 V, hence, after baseline correction, the EFV signal was reduced by 44% in the presence of NVP. Urea and uric acid (UA) are constituents of urine, hence they are present in wastewater samples. Therefore, the effects of these endogenous reducing compounds on the EFV signal were also tested. Urea was not electroactive in the chosen experimental conditions; hence it did not affect the EFV signal. Although UA was electroactive in the chosen potential window (E_p^a = 0.500 V), it did not also affect the EFV signal. Overall, the CuC/oxiBNCNO/GCE sensor exhibited excellent selectivity for the detection of EFV in the presence of interfering species. Inserted images in Fig. 7D are the chemical structures of the studied interferent species.

3.9. Repeatability, stability, and reproducibility studies

The intra-repeatability study (same-day analysis) of CuC/oxi-BNCNO/GCE towards the detection of 10 μM EFV was carried out by running a DPV of the sensor every 10 min and the data was represented in a form of a bar graph in Fig. 8A. The relative standard deviation (RSD) of the five voltammograms obtained was 2.71%, indicating excellent data precision and repeatability of the sensor. Therefore, CuC/oxi-BNCNO/GCE can be used multiple times to detect EFV with good precision. The long-term stability of the sensor was tested by employing the same electrode to detect EFV for a month (30 days). Between day 1 and day 6, the EFV signal decreased by only 1.52%. On day 30, the sensor was able to retain 95% of its original signal (Fig. 8B). To evaluate the

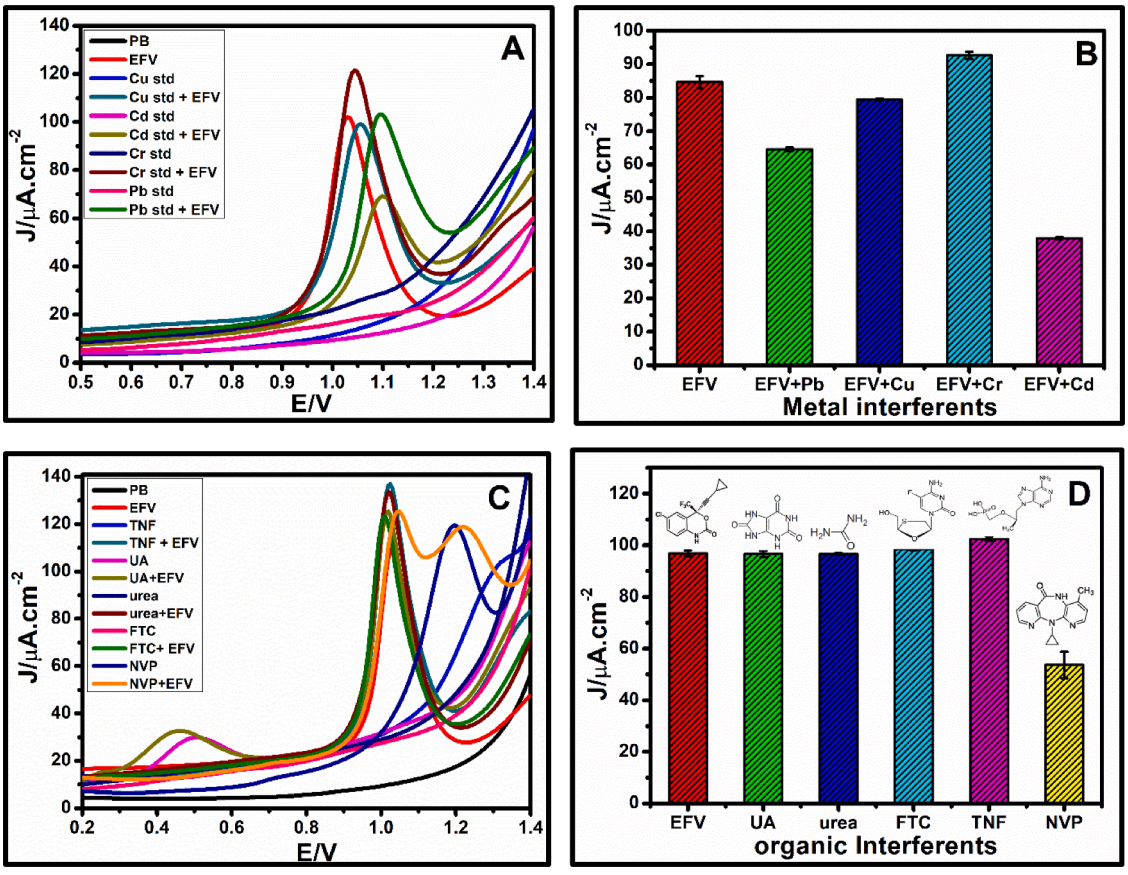

Fig. 7. DPV (A) and the corresponding bar graph (B) of 10μM EFV in the presence of 500μM of Pb, Cu, Cr and Cd. DPV (C) and a corresponding bar graph (D) of 10μM EFV in the presence of 100μM of UA, urea, FTC, TNF and NVP.

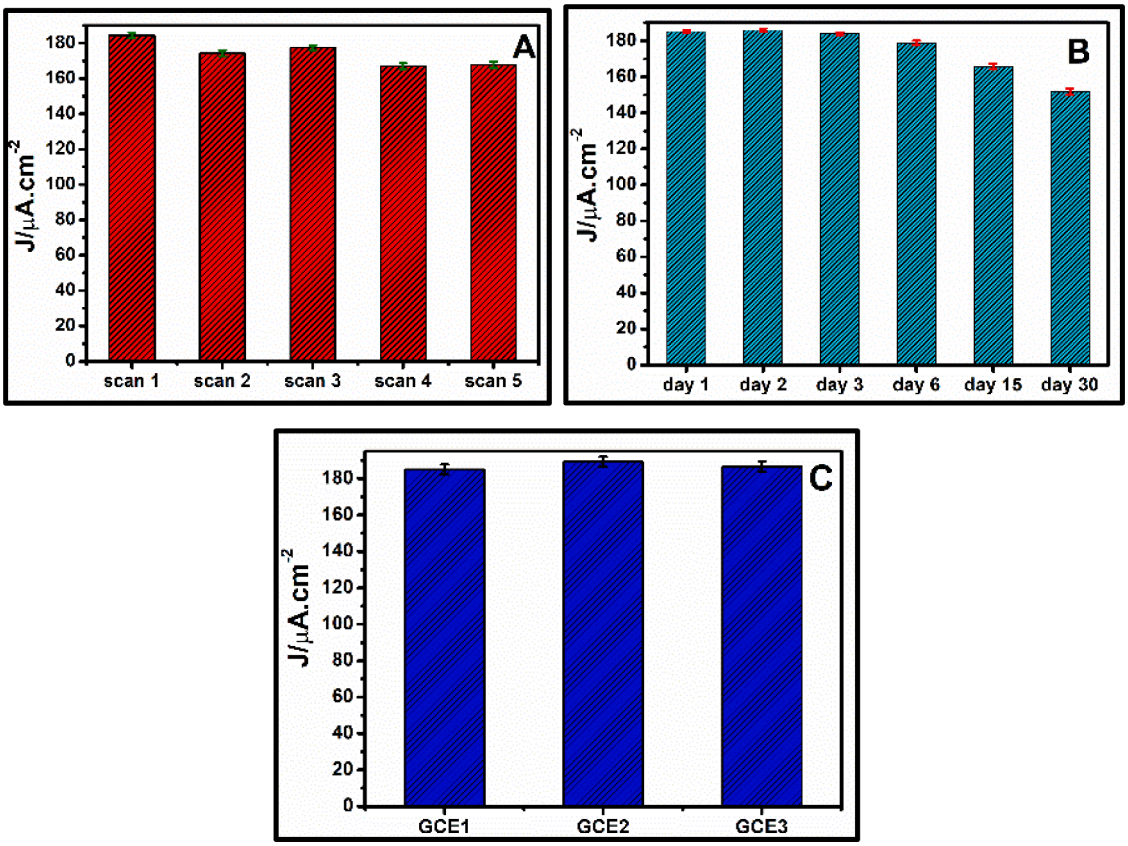

Fig. 8. Repeatability, stability, and reproducibility of the CuC/oxi-BNCNO/GCE sensor towards the detection of 10 μM EFV.

reproducibility of the sensor, three electrodes prepared in the same manner were employed, and their responses are presented in Fig. 8C. The acceptable precision and reproducibility of the three electrodes were demonstrated by an RSD of 0.82%.

3.10. Analytical applicability of CuC/oxi-BNCNO/GCE voltammetric sensor in real wastewater samples

Since EFV and most ARV commonly occur in μg L^{-1} concentrations in wastewater and surface water samples [12–15,19]; well within the detection capability of our methods, the developed method was employed for the detection of EFV in drinking water (tap water) and wastewater influent and effluent of the city of Cape Town, South Africa. Additionally, the sensor was also tested for the detection of EFV in the Atripla tablet, which is an ARV solid dose formulation containing EFV, FTC and TNF. The details of how the real samples were prepared and analysed are described in the experimental methods section. Due to the matrix effect in wastewater samples and Atripla tablets, the standard addition method was employed for the analysis and evaluation of the accuracy of the method. The sensors response in real samples are summarised in Tables 5 and 6. Extrapolating the linear graphs of the real samples to $y = 0$, the concentration of EFV in drinking water, wastewater influent and effluent and the Atripla tablet were found to be 0.00212, 0.151, 0.365, 1.91 μM, respectively. The percentage recoveries (R%) were also determined using Eq. (19) to evaluate the accuracy of the developed method.

$$R\% = \frac{C_{spiked} - C_{unspiked}}{C_{added}} \times 100 \quad (19)$$

where $C_{unspiked}$ is the concentration of the unknown in the real sample, C_{added} is the added known concentration of the stock and C_{spiked} is the $C_{unspiked} + C_{added}$ in the presence of the matrix. As summarised in Tables 5 and 6, the recovery percentages for different real samples spiked with different concentrations of EFV were between 97.8 1.2% and 109.6 1.5%. This demonstrates the excellent accuracy of the developed method for the detection of EFV in various real samples. This

Table 5
Voltammetric determination of EFV in various samples and their recovery% using the CuC/oxi-BNCNO/GCE sensor ($n = 3$).

Sample matrices	Concentration added (μM)	Concentration detected (μM)	RSD (%)	Recovery (%)
Tap/drinking water	0	0.00212	4.6	n/a
	0.1	0.101	3.5	98.9
	0.5	0.502	1.9	100.0
	1.0	0.995	3.4	99.3
Atripla tablet (600mg EFV declared)	0	1.91	2.0	n/a
	0.5	2.43	1.2	104.0
	5.0	6.80	1.2	97.8
	10.0	11.86	2.3	99.5

Table 6
Determination of EFV in wastewater influent and effluent using CuC/oxi-BNCNO/GCE sensor.

Sample matrices	Concentration added (μM)	Concentration detected (μM)	RSD (%)	Recovery (%)
Raw wastewater influent	0	0.151	4.8	n/a
	1	1.170	3.6	100.4
	5	5.630	1.5	109.6
	10	10.680	2.4	105.3
Wastewater effluent	0	0.365	2.1	n/a
	1	1.355	4.3	99.0
	5	5.300	6.4	98.7
	10	10.380	1.1	100.2

implies that the developed electroanalytical strategy is promising to distinguish EFV in the relevant matrices.

4. Conclusion

This study explored the fabrication and use of CuC/oxi-BNCNO/GCE as an electrode material for the voltammetric determination of EFV in wastewater and an ARV solid dose formulation. The CuC/oxi-BNCNO nanocomposite increased the estimated electroactive surface area of the GCE by a factor of three and the EFV electronic signal was enhanced by a factor of approximately four compared to a GCE. Moreover, the triple pulse electrosynthesis of copper flowers on the underlying nanostructured carbon surface resulted in well-dispersed, tightly adhered branched metal clusters on the CNO surface. On the developed sensing platform, EFV underwent irreversible oxidation which was diffusion controlled. During pH studies, the electronic signal of EFV shifted cathodically and increased until pH 8, then further decreased up to pH 12. The pH of wastewater is between 6 and 8, hence this pH is suitable for the intended study. Scan rate studies of EFV revealed important parameters such as D, α, k, and E^0. During the calibration study, the oxidation signal of EFV increased linearly with increasing concentration from 0.01 to 1 μM and 0.5 to 20 μM with LOD and LOQ of 1.2 nM and 3.97 nM, respectively. An interferent study showed that 50-fold of Pb^{2+} and Cd^{2+} affect the EFV signal, however, metal ions are unlikely to exist at such concentrations in water resources. The structurally similar NVP molecule has similar electrochemistry to EFV, hence its presence at high concentrations slightly affected the signal of EFV. Therefore, some redesign of the surface to include possible bimetallic dual deposition may be required to address this, being of interest in our group going forward. Overall, the newly developed method shows excellent behaviour and proven applicability for the determination of this important antiretroviral molecule in environmental and pharmaceutical samples.

CRediT authorship contribution statement

K.V. Mokwebo: Methodology, Investigation, Data curation, Visualization, Writing – original draft. **E. Murphy:** Methodology, Investigation. **S.K. Guin:** Conceptualization, Data curation, Visualization, Formal analysis, Writing – review & editing. **A. Camisasca:** Methodology, Resources. **S. Giordani:** Conceptualization, Resources. **C. Breslin:** Conceptualization, Funding acquisition. **E.I. Iwuoha:** Conceptualization, Supervision, Funding acquisition, Writing – review & editing. **E. Dempsey:** Conceptualization, Supervision, Funding acquisition, Project administration, Writing – review & editing.

Declaration of Competing Interest

The authors declare that they have no known competing financial interests or personal relationships that could have appeared to influence the work reported in this paper.

Data availability

Data will be made available on request.

Acknowledgment

The authors wish to express their gratitude to the Irish Research Council New Foundations Project (IRC/NF/2019/Dempsey), Water Research Commission (WRC) of South Africa: Sense and Purify (Spy) Project Grant (REF WRC C2019/2020–0008) under the EU Horizon 2020 ERA-Net Cofund Programme and the National Research Foundation (NRF) of South Africa: South African Research Chair Initiative (SARChI) Grant (REF 85102) for NanoElectrochemistry and Sensor Technology, for funding. Drs. Guin and Dempsey wish to acknowledge Enterprise Ireland and the European Union's Horizon 2020 Research and Innovation Programme under the Marie Skłodowska-Curie Career FIT PLUS Grant Agreement No. 847402. We also acknowledge Dr. Vasily Lebedev for HRSEM analysis at the Bernel Institute University of Limerick, Ireland.

Supplementary materials

Supplementary material associated with this article can be found, in the online version, at doi:10.1016/j.electacta.2023.142639.

References

[1] World Health Organisation (WHO). (2022). Global HIV programme: HIV data and statistics. Retrieved from https://www.who.int/teams/global-hiv-hepatitis-and-stisprogrammes/hiv/strategic-information/hiv-data-and-statistics. Accessed 31 May 2023.
[2] World Health Organisation (WHO) (2022). The global health observatory: reported number of people receiving antiretroviral therapy. Retrieved from https://www.who.int/data/gho/data/indicators/indicator-details/GHO/reported-number-of-people-receiving-antiretroviral-therapy. Accessed 31 May 2023.
[3] B.J. E.ckhardt, R.M. G.ulick, J. Cohen, W.G. Powderly, S.M. Opal, Drugs for HIV infection: emtricitabine, in: Infectious Diseases, 4th Ed., 2, Elsevier, 2017, pp. 1293–1308, e2.
[4] World health Organization Public Assessment Reports (WHOPAR). (2007). Efavirenz 600mg tablets (Ranbaxy) (Report No HA306/01/2007). Retrieved from https://extranet.who.int/pqweb/sites/default/files/documents/HA306Part6v1.pdf. Accessed 20 May 2023.
[5] K.V. Mokwebo, S.F. Douman, O.V. U.huo, K.C. Januarie, M. Oranzie, E.I. Iwuoha, Electroanalytical sensors for antiretroviral drugs determination in pharmaceutical and biological samples: a review, J. Electroanal. Chem. 920 (2022) 116621–116650.
[6] P.F. Wang, A. Neiner, E.D. Kharasch, Efavirenz metabolism: influence of polymorphic CYP2B6 variants and stereochemistry, Drug Metab. Dispos. 47 (2019) 1195–1205.
[7] A.M. Margolis, H. Heverling, P.A. Pham, A. Stolbach, A review of the toxicity of HIV medications, J. Med. Toxicol. 10 (2014) 26–39.
[8] M. Desai, G. Iyer, R. Dikshit, Antiretroviral drugs: critical issues and recent advances, Indian J. Pharmacol. 44 (2012) 288–298.
[9] V. Perrone, D. Cattaneo, S. Radice, D. Sangiorgi, A.B. Federici, M.R. Gismondo, et al., Impact of therapeutic drug monitoring of antiretroviral drugs in routine clinical management of patients infected with human immunodeficiency virus and related health care costs: a real-life study in a large cohort of patients, ClinicoEconomics and Outcomes Research CEOR 6 (2014) 341–348.
[10] S. Aftab, S. Kurbanoglu, G. Ozcelikay, N.K. Bakirhan, A. Shah, S.A. Ozkan, Carbon quantum dots co-catalyzed with multiwalled carbon nanotubes and silver nanoparticles modified nanosensor for the electrochemical assay of anti-HIV drug Rilpivirine, Sens. Actuators B. 285 (2019) 571–583.
[11] M. Jocelyn, M. Augustin, M. Adelard, Development and validation of HPLC methods for simultaneous analysis of 6 antiretrovirals in pharmaceutical formulations, J. Analalytical Pharmarceutical Res. 8 (2019) 200–207.
[12] C. Schoeman, M. Dlamini, O. Okonkwo, The impact of a wastewater treatment works in Southern Gauteng, South Africa on efavirenz and nevirapine discharges into the aquatic environment, Emerg. Contam. 3 (2017) 95–106.
[13] O.A. A.bafe, J. Späth, J. Fick, S. Jansson, C. Buckley, A. Stark, et al., LC-MS/MS determination of antiretroviral drugs in influents and effluents from wastewater treatment plants in KwaZulu-Natal, South Africa, Chemosphere 200 (2018) 660–670.
[14] K. K'oreje, L. Vergeynst, D. Ombaka, P. De Wispelaere, M. Okoth, H. Van Langenhove, et al., Occurrence patterns of pharmaceutical residues in wastewater, surface water and groundwater of Nairobi and Kisumu city, Kenya, Chemosphere 149 (2016) 238–244.
[15] T.T. Mosekiemang, M.A. Stander, A. de Villiers, Simultaneous quantification of commonly prescribed antiretroviral drugs and their selected metabolites in aqueous environmental samples by direct injection and solid phase extraction liquid chromatography-tandem mass spectrometry, Chemosphere 220 (2019) 983–992.
[16] C. Schoeman, M. Mashiane, M. Dlamini, O. Okonkwo, Quantification of selected antiretroviral drugs in a wastewater treatment works in South Africa using GC-TOFMS, J. Chromatogr. Sep. Tech. 6 (2015) 1–7.
[17] N.Y. M.lunguza, S. Ncube, P.N. Mahlambi, L. Chimuka, L.M. Madikizela, Determination of selected antiretroviral drugs in wastewater, surface water and aquatic plants using hollow fibre liquid phase microextraction and liquid chromatography-tandem mass spectrometry, J. Hazard. Mater. 382 (2020), 121067-121077.
[18] T.P. Wood, C.S. D.uvenage, E. Rohwer, The occurrence of anti-retroviral compounds used for HIV treatment in South African surface water, Environ. Pollut. 199 (2015) 235–243.
[19] C. Rimayi, D. Odusanya, J.M. Weiss, J. de Boer, L. Chimuka, Contaminants of emerging concern in the hartbeespoort dam catchment and the uMngeni river estuary 2016 pollution incident, South Africa, Sci. Total Environ. 627 (2018) 1008–1017.

[20] M. Wooding, E.R. Rohwer, Y. Naudé, Determination of endocrine disrupting chemicals and antiretroviral compounds in surface water: a disposable sorptive sampler with comprehensive gas chromatography–time-of-flight mass spectrometry and large volume injection with ultra-high performance liquid chromatography–tandem mass spectrometry, J. Chromatogr. A 1496 (2017) 122–132.

[21] C. Swanepoel, H. Bouwman, R. Pieters, C. Bezuidenhout (2015). Presence, concentrations and potential implications of HIV-anti-retrovirals in selected water resources in South Africa (WRC Report No. 2144/1/14), Water Research Commission. Retrieved from https://wrcwebsite.azurewebsites.net/wp-content/uploads/mdocs/2144-1-14.pdf. Accessed 31 May 2023.

[22] E.S Martins, J.A. Oliveira, T.B. Franchin, B.C.U. Silva, C.D. Cândido, R.G. Peccinini, Simple and rapid method by ultra high-performance liquid chromatography (UHPLC) with ultraviolet detection for determination of efavirenz in plasma: application in a preclinical pharmacokinetic study, J. Chromatogr. Sci. 57 (2019) 874–880.

[23] A.A. Castro, M.V. de Souza, N.A. Rey, P.A. Farias, Determination of efavirenz in diluted alkaline electrolyte by cathodic adsorptive stripping voltammetry at the mercury film electrode, J. Braz. Chem. Soc. 22 (2011) 1662–1668.

[24] B. Dogan-Topal, B. Uslu, S.A. Ozkan, Voltammetric studies on the HIV-1 inhibitory drug Efavirenz: the interaction between dsDNA and drug using electrochemical DNA biosensor and adsorptive stripping voltammetric determination on disposable pencil graphite electrode, Biosens. Bioelectron. 24 (2009) 2358–2364.

[25] M. Raj, P. Gupta, N. Thapliyal, R.N. G.oyal, A novel hybrid nano-composite grafted electrochemically reduced graphene oxide based sensor for sensitive determination of Efavirenz, Electroanalysis 29 (2017) 456–465.

[26] N. Thapliyal, N.S. Osman, H. Patel, R. Karpoormath, R.N. Goyal, T. Moyo, et al., NiO–ZrO_2 nanocomposite modified electrode for the sensitive and selective determination of efavirenz, an anti-HIV drug, RSC Adv. 5 (2015) 40057–40064.

[27] K. Mthiyane, G.E. Uwaya, M.A. Jordaan, S. Kanchi, K. Bisetty, Insights into the design of an enzyme free sustainable sensing platform for efavirenz, Catalysts 12 (2022) 830–846.

[28] N.M. Xhakaza, R. Chokkareddy, G.G. Redhi, Ionic liquid based electrochemical sensor for the detection of Efavirenz, J. Mol. Liq. (2022) 120444–120452.

[29] J.P. Bartolome, A. Fragoso, Electrochemical detection of nitrite and ascorbic acid at glassy carbon electrodes modified with carbon nano-onions bearing electroactive moieties, Inorg. Chim. Acta 468 (2017) 223–231.

[30] A. Camisasca, A. Sacco, R. Brescia, S. Giordani, Boron/nitrogen-codoped carbon nano-onion electrocatalysts for the oxygen reduction reaction, ACS Appl. Nano Mater. 1 (2018) 5763–5773.

[31] N. Keller, N.I. Maksimova, V.V. R.oddatis, M. Schur, G. Mestl, Y.V. B.utenko, et al., The catalytic use of onion-like carbon materials for styrene synthesis by oxidative dehydrogenation of ethylbenzene, Angew. Chem. Int. Ed. 41 (2002) 1885–1888.

[32] O. Mykhailiv, H. Zubyk, M.E. Plonska-Brzezinska, Carbon nano-onions: unique carbon nanostructures with fascinating properties and their potential applications, Inorg, Chim. Acta 468 (2017) 49–66.

[33] M. Olariu, A. Arcire, M.E. Plonska-Brzezinska, Controlled trapping of onion-like carbon (OLC) via dielectrophoresis, J. Electron. Mater. 46 (2017) 443–450.

[34] A. Shaikh, B.K. Singh, D. Mohapatra, S. Parida, Nitrogen-doped carbon nano-onions as a metal-free electrocatalyst, Electrocatalysis 10 (2019) 222–231.

[35] E. Sohouli, A.H. Keihan, F. Shahdost-Fard, E. Naghian, M.E. Plonska-Brzezinska, M. Rahimi-Nasrabadi, et al., A glassy carbon electrode modified with carbon nanoonions for electrochemical determination of fentanyl, Mater. Sci. Eng. C 110 (2020), 110684-110694.

[36] L.L. Sikeyi, T.D. Ntuli, T.H. Mongwe, N.W. Maxakato, N.J. Coville, M.S. Maubane-Nkadimeng, Platinum nanoparticles loaded on pristine and boron oxide modified carbon nano-onions for enhanced ammonia electrooxidation in alkaline direct ammonia fuel cells, J. Electroanal. Chem. 917 (2022) 116411–116423.

[37] S. Xu, M. Wang, G. Saranya, N. Chen, L. Zhang, Y. He, et al., Pressure-driven catalyst synthesis of Co-doped Fe_3C@ carbon nano-onions for efficient oxygen evolution reaction, Appl. Catal. B 268 (2020), 118385-118395.

[38] J.C. Zuaznabar-Gardona, A. Fragoso, A wide-range solid state potentiometric pH sensor based on poly-dopamine coated carbon nano-onion electrodes, Sens. Actuators B 273 (2018) 664–671.

[39] H.M. Y.adav, J.J. Lee, One-pot synthesis of copper nanoparticles on glass: applications for non-enzymatic glucose detection and catalytic reduction of 4-nitrophenol, J. Solid State Electrochem. 23 (2019) 503–512.

[40] P. Balasubramanian, M. Velmurugan, S.M. Chen, K.Y. Hwa, Optimized electrochemical synthesis of copper nanoparticles decorated reduced graphene oxide: application for enzymeless determination of glucose in human blood, J. Electroanal. Chem. 807 (2017) 128–136.

[41] V. Sudha, G. Murugadoss, R. Thangamuthu, Structural and morphological tuning of Cu-based metal oxide nanoparticles by a facile chemical method and highly electrochemical sensing of sulphite, Sci. Rep. 11 (2021) 1–12.

[42] P. Balasubramanian, T. Balamurugan, S.M. Chen, T.W. Chen, T. Sathesh, Rational design of Cu@Cu_2O nanospheres anchored B, N co-doped mesoporous carbon: a sustainable electrocatalyst to assay eminent neurotransmitters acetylcholine and dopamine, ACS Sustain. Chem. Eng. 7 (2018) 5669–5680.

[43] S.K. Guin, H. Sharma, S.K. Aggarwal, Electrosynthesis of lead nanoparticles on template free gold surface by potentiostatic triple pulse technique, Electrochim. Acta 55 (2010) 1245–1257.

[44] S.K. Guin, J.S. Pillai, A.S. Ambolikar, A. Saha, S.K. Aggarwal, Template-free electrosynthesis of gold nanoparticles of controlled size dispersion for the determination of lead at ultratrace levels, RSC Adv. 3 (2013) 17977–17988.

[45] S.K. G.uin, P. Knittel, S. Daboss, A. Breusow, C. Kranz, Template-and additive-free electrosynthesis and characterization of spherical gold nanoparticles on hydrophobic conducting polydimethylsiloxane, Chem. Asian J. 12 (2017) 1615–1624.

[46] S.K. Guin, S.K. Aggarwal, Prospective use of the potentiostatic triple pulse strategy for the template-free electrosynthesis of metal nanoparticles, RSC Adv. 4 (2014) 55349–55353.

[47] S.K. Guin, R. Phatak, J.S. Pillai, A. Sarkar, S.K. Aggarwal, A mechanistic study on the effect of a surface protecting agent on electrocrystallization of silver nanoparticles, RSC Adv. 4 (2014) 59927–59935.

[48] B. Scharifker, G. Hills, Theoretical and experimental studies of multiple nucleation, Electrochim. Acta 28 (1983) 879–889.

[49] M. Mirkin, A. Nilov, Three-dimensional nucleation and growth under controlled potential, J. Electroanal. Chem. Interfacial Electrochem. 283 (1990) 35–51.

[50] L. Heerman, A. Tarallo, Theory of the chronoamperometric transient for electrochemical nucleation with diffusion-controlled growth, J. Electroanal. Chem. 470 (1999) 70–76.

[51] A. Camisasca, S. Giordani, Carbon nano-onions in biomedical applications: promising theranostic agents, Inorganica Chim Acta 468 (2017) 67–76.

[52] L.R. Cumba, A. Camisasca, S. Giordani, R.J. Forster, Electrochemical properties of screen-printed carbon nano-onion electrodes, Molecules 25 (2020) 3884.

[53] E. Sohouli, M. Ghalkhani, T. Zargar, Y. Joseph, M. Rahimi-Nasrabadi, F. Ahmadi, et al., A new electrochemical aptasensor based on gold/nitrogen-doped carbon nano-onions for the detection of Staphylococcus aureus, Electrochim. Acta 403 (2022), 139633.

[54] E. Sohouli, F. Shahdost-Fard, M. Rahimi-Nasrabadi, M.E. P.lonska-Brzezinska, F. Ahmadi, Introducing a novel nanocomposite consisting of nitrogen-doped carbon nano-onions and gold nanoparticles for the electrochemical sensor to measure acetaminophen, J. Electroanal. Chem. 871 (2020), 114309-114320.

[55] M.H. G.hanbari, Z. Norouzi, A new nanostructure consisting of nitrogen-doped carbon nanoonions for an electrochemical sensor to the determination of doxorubicin, Microchem. J. 157 (2020), 105098-105108.

[56] E.P. Randviir, A cross examination of electron transfer rate constants for carbon screen-printed electrodes using electrochemical impedance spectroscopy and cyclic voltammetry, Electrochim. Acta 286 (2018) 179–186.

[57] R.S. Nicholson, I. Shain, Theory of stationary electrode polarography. Single scan and cyclic methods applied to reversible, irreversible, and kinetic systems, Anal. Chem. 36 (1964) 706–723.

[58] E. Laviron, L. Roullier, General expression of the linear potential sweep voltammogram for a surface redox reaction with interactions between the adsorbed molecules: applications to modified electrodes, J. Electroanal. Chem. Interfacial Electrochem. 115 (1980) 65–74.

[59] J. Wang, J. Schultze, Analytical electrochemistry, Angew. Chem. Engl. Ed. 35 (1996) 1998, 1998.

[60] F.W.P. Ribeiro, R.C. de Oliveira, A.G. de Oliveira, R.F. Nascimento, H. Becker, P. de Lima-Neto, et al., Electrochemical sensing of thiabendazole in complex samples using boron-doped diamond electrode, J. Electroanal. Chem. 866 (2020), 114179-114187.

[61] Y. Wang, G. Zhu, D. Wang, M. Huang, J. Yang, J. Liu, One-step synthesis of ultrafine silver-decorated polyaniline nanowire arrays for trace analysis of sulfamethoxazole, Electrochim. Acta 436 (2022), 141434-141446.

[62] M.B. G.holivand, E. Ahmadi, M. Haseli, A novel voltammetric sensor for nevirapine, based on modified graphite electrode by MWCNs/poly (methylene blue)/gold nanoparticle, Anal. Biochem. 527 (2017) 4–12.

[63] B.H. Pour, N. Haghnazari, F. Keshavarzi, E. Ahmadi, B.R. Zarif, A sensitive sensor based on molecularly imprinted polypyrrole on reduced graphene oxide modified glassy carbon electrode for nevirapine analysis, Anal. Methods. 13 (2021) 4767–4777.

[64] European Medicine Agency (2017). Efavirenz/emtricitabine/tenofovir disoproxil mylan (EMA Report No. EMA/CHMP/630402/2017). European Union. Retrieved from https://www.ema.europa.eu/en/documents/assessment-report/efavirenz/emtricitabine/tenofovir-disoproxil-mylan-epar-public-assessment-report_en.pdf. Accessed 31 May 2023.

[65] J.A. de Aquino Ribeiro, L.M.M. de Campos, R.J. Alves, G.P. Lages, G.A. Pianetti, Efavirenz related compounds preparation by hydrolysis procedure: setting reference standards for chromatographic purity analysis, J. Pharm. Biomed. Anal. 43 (2007) 298–303.

[66] M.B. Maurin, S.M. R.owe, K. Blom, M.E. Pierce, Kinetics and mechanism of hydrolysis of Efavirenz, Pharm. Res. 19 (2002) 517–521.

[67] M. Kurmi, A. Sahu, D.K. Singh, I.P. Singh, S. Singh, Stability behaviour of antiretroviral drugs and their combinations. 8: characterization and in-silico toxicity prediction of degradation products of efavirenz, J. Pharm. Biomed. Anal. 148 (2018) 170–181.

[68] L.A. Currie, Nomenclature in evaluation of analytical methods including detection and quantification capabilities (IUPAC recommendations 1995), Pure Appl. Chem. 67 (1995) 1699–1723.

[69] S. Allahverdiyeva, P.T. Pınar, Y. Yardım, Z. Şentürk, First report for the electrochemical investigation of a new HIV integrase inhibitor dolutegravir: its voltammetric determination in tablet dosage forms and human urine using a boron-doped diamond electrode, Diam. Relat. Mater. 114 (2021) 108332–108340.